Supplementary Information

Seasonal sea-ice in the Arctic's last ice area during the Early Holocene

Authors: Henrieka Detlef[1,2*], Matt O'Regan[3], Christian Stranne[3], Mads Mørk Jensen[4], Marianne Glasius[4,2], Thomas M. Cronin[5], Martin Jakobsson[3], Christof Pearce[1,2]

Affiliations:

[1]Department of Geoscience, Aarhus University; Aarhus, Denmark.

[2]Arctic Research Centre, Aarhus University; Aarhus, Denmark.

[3]Department of Geological Sciences, Stockholm University; Stockholm, Sweden.

[4]Department of Chemistry, Aarhus University; Aarhus, Denmark.

[5]Florence Bascom Geoscience Center, U.S. Geological Survey, Reston, VA, USA

*Corresponding author. Email: henrieka.detlef@geo.au.dk

1. Supplementary Methods

1.1 Normalization of biomarker concentrations to TOC versus sediment mass

Two common practices in sea-ice biomarker research are normalization of biomarker concentrations to the extracted sediment mass and/or TOC[1]. While normalizing to TOC may reduce the bias related to degradation of biomarkers depending on the bottom water/sedimentary redox conditions[1], non-marine sources (e.g. terrestrial, lacustrine) and refractory organic matter from terrestrial/geological sources can affect the TOC record. For 12-GC and 14-GC, the choice of normalization does not make a significant difference in biomarker trends (Supplementary Fig. 1). Thus, biomarkers normalized to sediment mass have been interpreted alongside TOC content to make inferences about Holocene sea-ice dynamics in the southern Lincoln Sea.

1.2 Agassiz MAAT from pre-industrial

The published record of MAAT at Agassiz Ice Cap is normalized to 1750 CE[2]. Projections of Arctic atmospheric temperatures under future warming scenarios, on the other hand, are typically reported as anomalies compared to the pre-industrial period (1850-1900 CE). Thus, the Agassiz Ice Cap MAAT record was adjusted by the temperature difference (ΔT = 0.88 °C) between 1750 CE (0.6 °C) and the average of 1850-1900 CE (1.48 °C). MAAT at 1750 CE is not equal to zero, as the data represents 25-year bins. Thus, ΔT is actually the difference between 1750 ± 12.5 CE and 1850-1900 ± 12.5 CE. To derive the MAAT at Agassiz Ice Cap compared to pre-industrial, ΔT was subtracted from the published values for MAAT and the upper and lower values of the 2σ uncertainty, respectively.

2. Supplementary Discussion

2.1 Additional climate mechanisms and their impact on the Early Holocene sea-ice cover in the Lincoln Sea

Sea-ice variability through time is the result of external forcing and internal variability, with atmospheric temperatures, independent of their causes (solar insolation, atmospheric greenhouse gas concentrations), exerting the dominant forcing[3,4]. Additional mechanisms affecting Arctic sea-ice cover are, amongst others, the surface ocean freshwater budget, stratification, and atmospheric/oceanic circulation[3,5].

Following deglaciation, the Greenland ice sheet[6] and other ice sheets bordering the Arctic Ocean[7] experienced a rapid reduction in height, resulting in increased freshwater input to the Arctic Ocean during the Early Holocene[8,9]. This might have strengthened the surface ocean stratification[9], resulting in a shallower and fresher mixed layer. Freshening of the mixed layer and strengthening of the halocline limits the transfer of heat between the cold surface waters and the warmer intermediate waters of Atlantic origin, promoting sea-ice formation[10–13]. On the other hand, a shallower mixed layer and increased stratification also increases the uptake of heat in the open surface ocean during summer, delaying the autumn freeze up[3]. Additionally, meltwater discharge at the grounding zones of glaciers ending in an ice tongue has been shown to increase the turbulent mixing underneath the ice tongue[14–16], resulting in incorporation of modified Atlantic Water (AW) into the surface mixed layer, potentially causing (local) weakening of the surface ocean stratification due to input of warmer more saline AW. During the Early Holocene, benthic foraminiferal assemblages in the southern Lincoln Sea (12-GC and 14-GC), Sherard Osborn Fjord (Ryder19-07-PC1)[17], and Hall Basin (HLY03-01-05GC)[18,19] (Fig. 1, Fig. 4) indicate the presence of modified AW and lithological evidence from Sherard Osborn Fjord suggests that Ryder Glacier ended in an extensive ice tongue at the time[20], which might have caused enhanced up-mixing of AW. Thus, the net effect of increased freshwater input to the Arctic Ocean/the Lincoln Sea on Early Holocene sea-ice concentration is difficult to assess, and it is unclear if the increased freshwater budget dampened or amplified the effects of rising atmospheric temperatures on sea-ice in the Lincoln Sea.

In addition to the freshwater input, atmospheric/oceanic circulation might have affected the Early Holocene Arctic sea-ice concentration. Compared to the mid-to-late Holocene, the Early Holocene was characterized by a closed Nares Strait, as the confluent Innuitian and Greenland ice sheets blocked the flow from the Lincoln Sea to the northern Baffin Bay until ca. 8.3 cal ka BP[18]. An open/closed Nares Strait likely influences the export of MYI from the Lincoln Sea. Historically, the flow of ice through Nares Strait was limited by the formation of ice arches during winter[21]. In recent years, however, recurrent failure of these ice arches has been associated with enhanced ice volume flux through Nares Strait[22,23]. This suggests that unrestricted flow of ice through Nares Strait enhances the export of sea-ice from the Lincoln Sea, while a blocked Nares Strait might be associated with increased retention of MYI in the Lincoln Sea. During the Early Holocene, the ice saddle blocking Nares Strait might thus have counteracted the atmospheric temperature driven decline in the Lincoln Sea ice cover.

On the other hand, while the Nares Strait was blocked, sea-ice export through the Fram Strait was likely enhanced during the Early Holocene. Proxy records from the Arctic Ocean and North Atlantic suggest an atmospheric circulation pattern resembling that of a strongly positive mode of the Arctic Oscillation (AO) during the early Holocene[24–28]. During a positive AO mode, the Beaufort Gyre is weak or even vanishes, and the Transpolar Drift is strengthened and shifted to the West[29–31]. In terms of Arctic Ocean sea-ice transport, this causes divergence in the East Siberian Sea and convergence off Canada with enhanced export of sea-ice through the Fram Strait. The latter is also supported by modeling experiments, investigating the effects of Arctic gateways on sea-ice and surface ocean circulation[5]. An open Bering Strait (< 11 cal ka BP[32]) and a (partially) closed Canadian Arctic Archipelago[18,33] during the Early Holocene, suggests enhanced sea-ice volume transport through the Fram Strait[5]. Thus, even though the Nares Strait remained closed until ca. 8.3 cal ka BP[18], limiting the ability of multi-year ice to be flushed from the Lincoln Sea[22], other processes enhancing the export of sea-ice through Fram Strait, may have amplified the thermally driven Arctic Ocean sea-ice decline in the Early Holocene.

2.2 Biomarkers and TOC in modern surface sediments of the northern Nares Strait, southern Lincoln Sea, and Sherard Osborn Fjord

In addition to 12-GC and 14-GC, biomarker (HBI, brassicasterol) concentrations and TOC were analyzed in 15 multi-corer surface sediments (0-1 cm to 0-5 cm) from the northern Nares Strait (Hall Basin and Petermann Fjord), the southern Lincoln Sea, and Sherard Osborn Fjord (Fig. 4) (Supplementary table 7). The highest IP_{25} concentrations are observed in Hall Basin, outer Petermann Fjord, and the southern Lincoln Sea, while the lowest concentrations are present in Sherard Osborn Fjord, with absent IP_{25} at station 9, located closest to the ice tongue terminus (Fig. 4, Supplementary Fig. 2). Both Petermann Fjord (n=3) and Sherard Osborn Fjord (n=7), show decreasing IP_{25} concentrations from the fjord mouth to the ice tongue terminus (Supplementary Fig. 2). This might reflect a decrease in general productivity close to the glacial terminus and/or the influence of freshwater on IP_{25} production[34]. During the Ryder19 cruise, a freshwater lid was observed in the ice free Sherard Osborn Fjord, as a result of damming by thick sea-ice outside the fjord[35]. This effect might make Sherard Osborn Fjord more sensitive to the influence of freshwater on sympagic biomarker production, compared to Petermann Fjord, where sea-ice in Hall Basin typically clears out prior to the fjord[36], allowing freshwater to escape the fjord more easily. A decrease in productivity close to the glacial termini is supported by low TOC content in the inner part of Sherard Osborn and Petermann Fjord (Supplementary Fig. 2). On the other hand, brassicasterol concentrations are higher in the fjords compared to the southern Lincoln Sea and Hall Basin (Supplementary Fig. 2), which may indicate a different primary producer community composition inside the fjords compared to the open shelf sea. The P_BIP_{25} index shows highest values in the southern Lincoln Sea and lowest values in Petermann and Sherard Osborn Fjord (Supplementary Fig. 2), suggesting a longer sea-ice season in the Lincoln Sea compared to the adjacent fjord systems. In the fjords, however, the P_BIP_{25} index might be artificially low in relation to suppressed production of IP_{25} by enhanced freshwater input. P_BIP_{25} values of 0.6-0.8 in the southern Lincoln Sea are in line with seasonal to perennial sea-ice.

The multi-corer surface samples at station 12 and 13 (in close proximity to 14-GC) integrate the top 2 cm and 1 cm, respectively (Supplementary table 7). According to the sedimentation rates based on the age model presented in this manuscript (Fig. 6), the samples likely cover the last 650-750 years. Considering that times of perennial ice cover in the southern Lincoln Sea are marked by very low biomarker concentrations (Fig. 2), it is likely that the surface samples are biased towards times of a reduced sea-ice cover (e.g. the last decade) associated with a beginning shift from a perennial to a more mobile/seasonal sea-ice cover in the Lincoln Sea[22,37–39].

3. Supplementary Figures

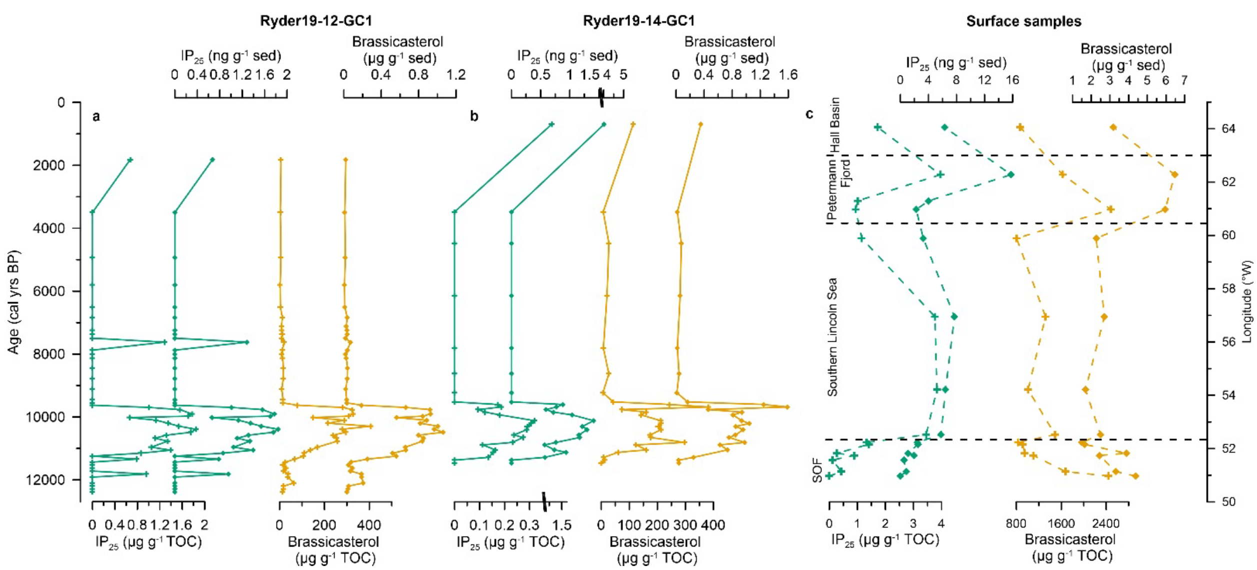

Supplementary Fig. 1. Biomarker concentrations normalized to TOC versus sediment mass. a IP_{25} (green) and brassicasterol (light brown) concentrations in 12-GC normalized to TOC (crosses) and extracted sediment mass (diamonds). **b** IP_{25} (green) and brassicasterol (light brown) concentrations in 14-GC normalized to TOC (crosses) and extracted sediment mass (diamonds). **c** Surface samples IP_{25} (green) and brassicasterol (light brown) normalized to TOC (crosses) and extracted sediment mass (diamonds).

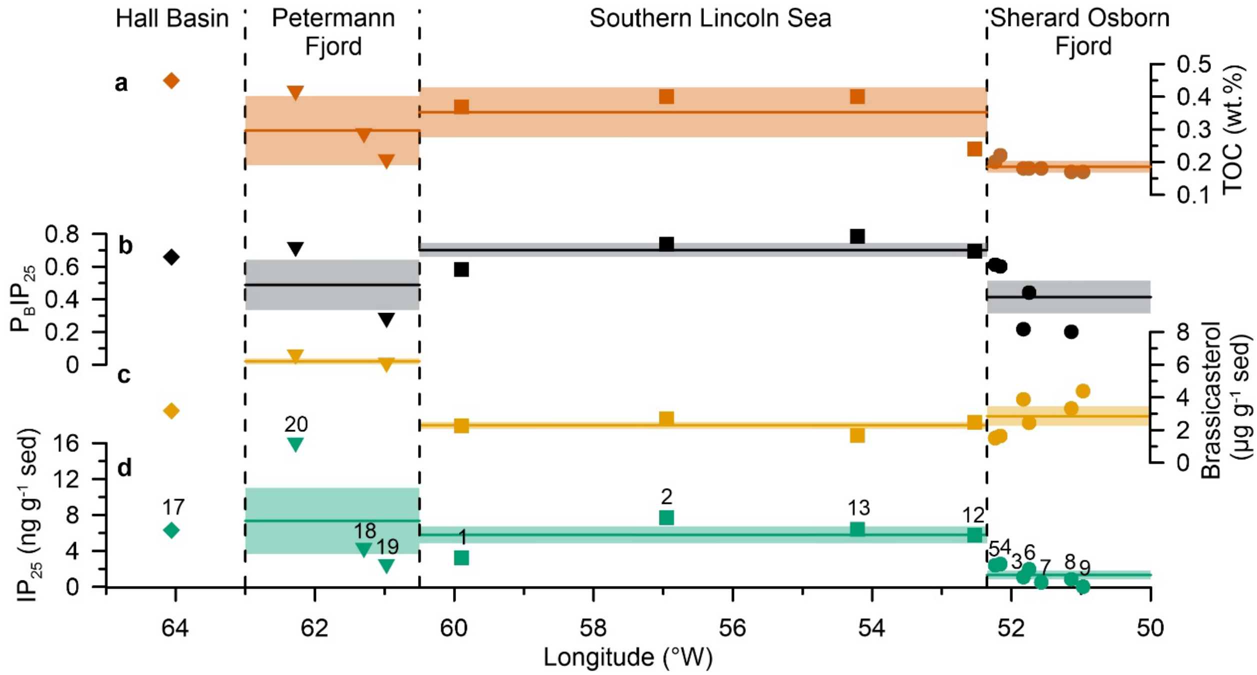

Supplementary Fig. 2. Biomarker concentrations and TOC in surface sediments from the Ryder19 cruise. a TOC (red-brown), **b** P_BIP_{25} (grey), **c** brassicasterol (orange), **d** IP_{25} (green) in surface sediments from the Hall Basin (diamond), Petermann Fjord (triangles), the southern Lincoln Sea (rectangles), and Sherard Osborn Fjord (dots), including the regional mean (solid line) and 1σ uncertainty envelope (shaded bar). The numbers correspond to the station numbers in Fig. 4.

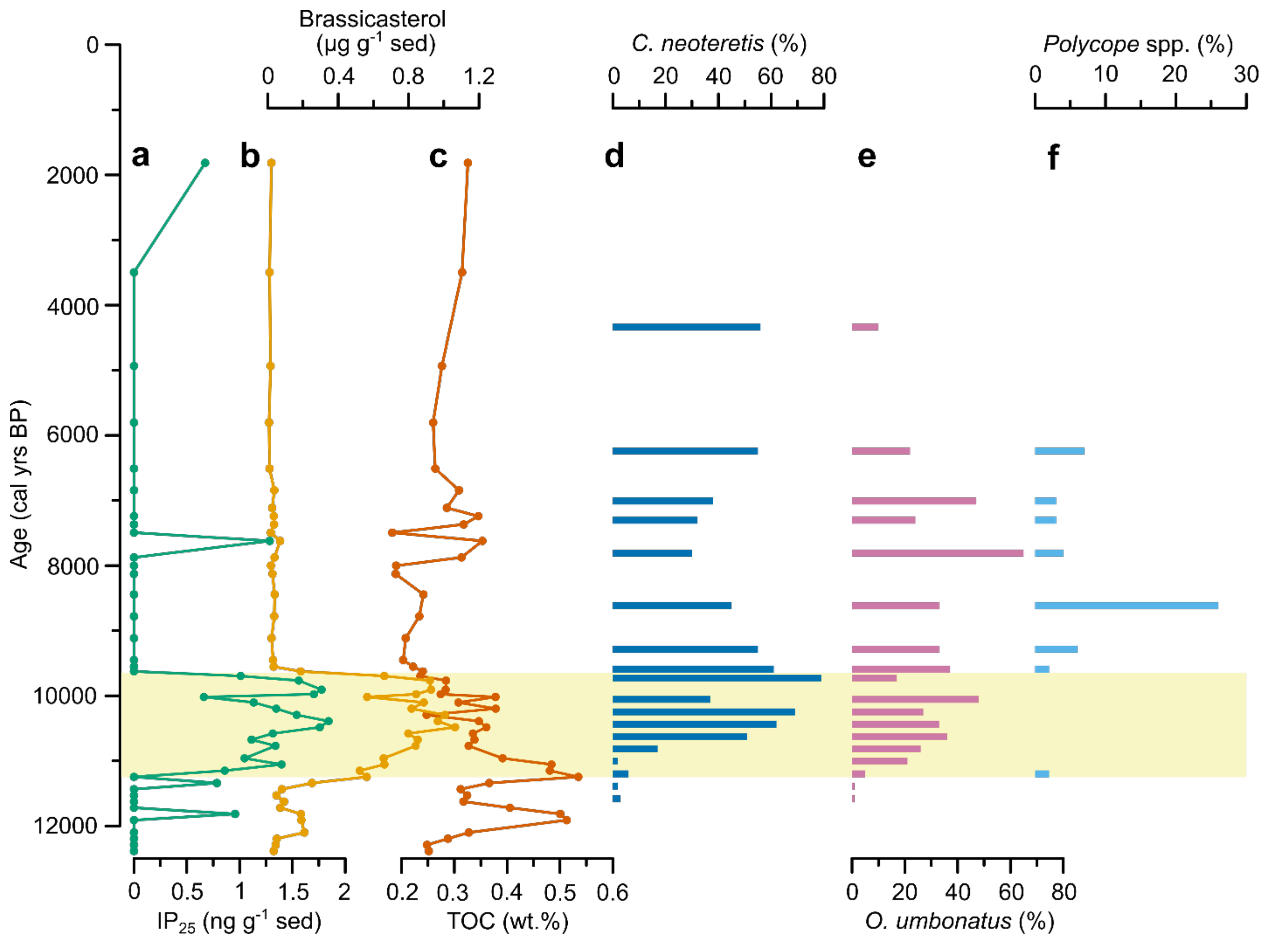

Supplementary Fig. 3. IP$_{25}$, Brassicasterol, TOC, and micropalontological assemblages at 12-GC. a IP$_{25}$ (green), **b** brassicasterol (orange), **c** TOC (red-brown), **d** abundance of *Cassidulina neoteretis* (blue), **e** *Oridorsalis umbonatus* (pink), and **f** *Polycope* spp. (light blue). The Early Holocene interval of seasonal sea-ice in the southern Lincoln Sea is marked with a light yellow horizontal bar.

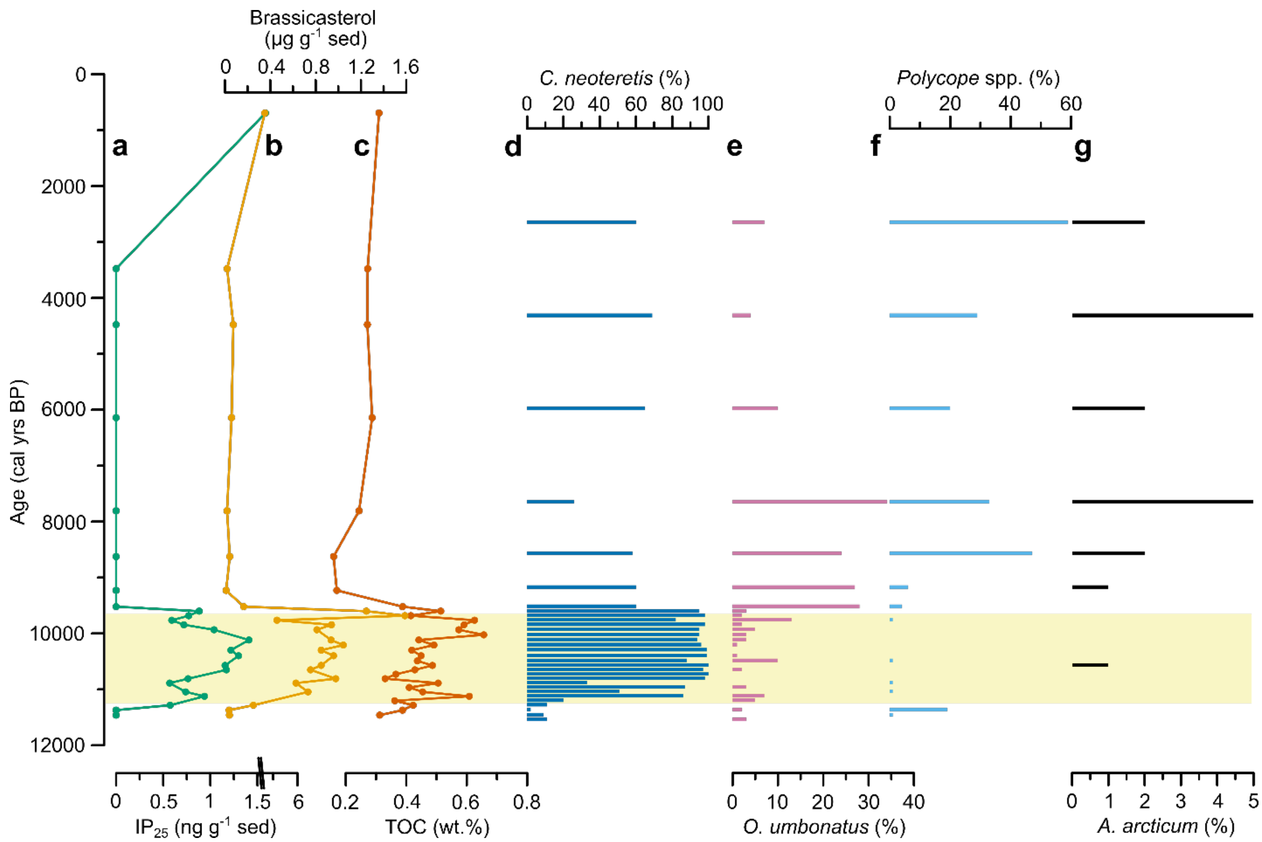

Supplementary Fig. 4. IP_{25}, Brassicasterol, TOC, and micropalontological assemblages at 14-GC. a IP_{25} (green), **b** brassicasterol (orange), **c** TOC (red-brown), **d** abundance of *Cassidulina neoteretis* (blue), **e** *Oridorsalis umbonatus* (pink), **f** *Polycope* spp. (light blue), and **g** *Acetabulastoma arcticum* (black). The Early Holocene interval of seasonal sea-ice in the southern Lincoln Sea is marked with a light yellow horizontal bar.

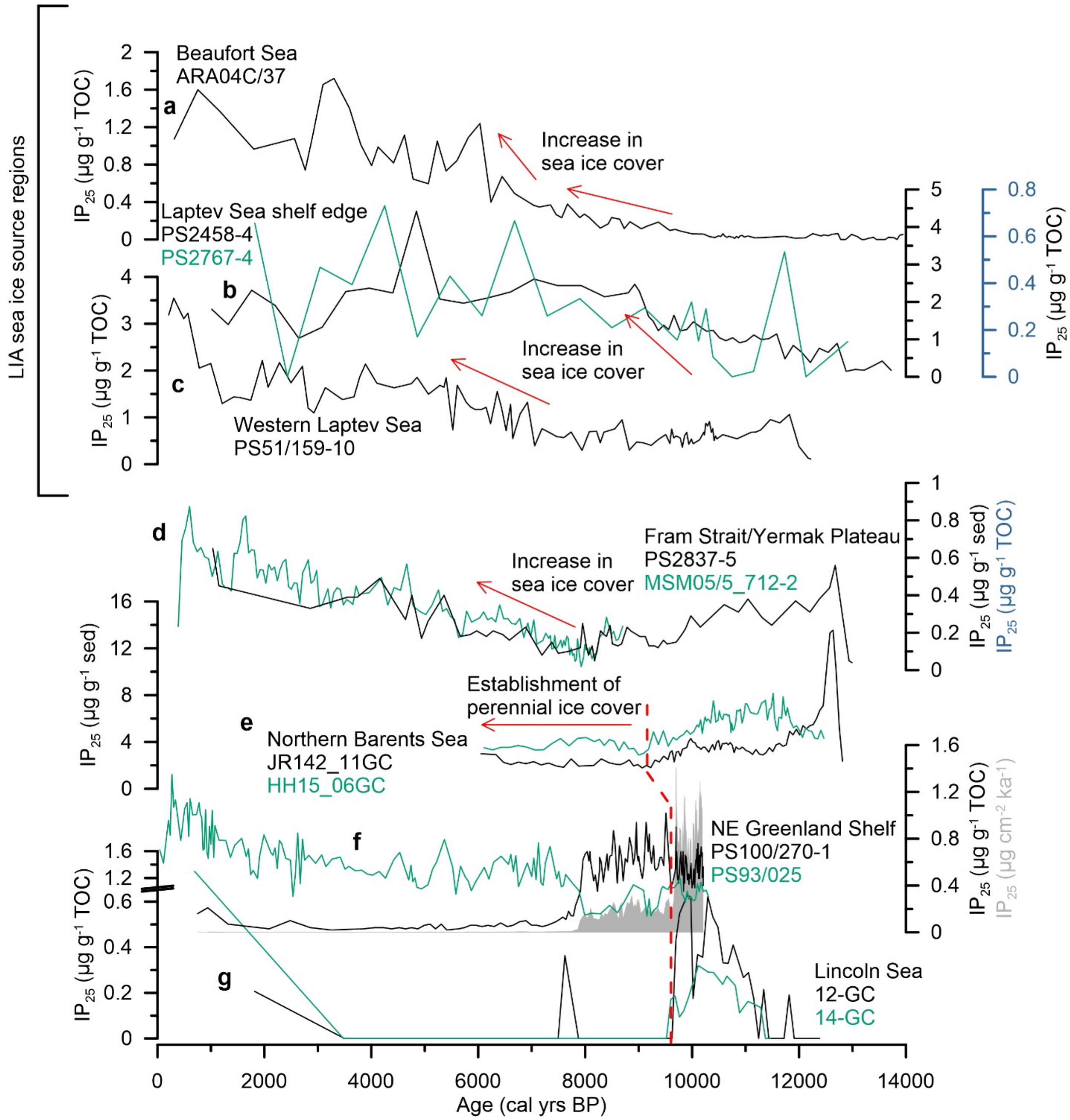

Supplementary Fig. 5. Holocene records of IP_{25} from across the Arctic Ocean and the Greenland Sea. a IP_{25} from ARA04C/37[47] from the Beaufort Sea, **b** IP_{25} from PS2458-4[45] (black) and PS2767-4[46] (green) from the Laptev Sea shelf edge, **c** IP_{25} from PS51/159-10[44] (black) in the western Laptev Sea, **d** IP_{25} from PS2837-5[42] (black) and MSM05/5_712-2[43] (green) in the eastern Fram Strait, **e** IP_{25} from JR142-11GC (black) and HH15-06GC (green) from the northernmost Barents Sea[10], **f** IP_{25} concentration (black) and fluxes (grey shaded area) from PS100/270-1[40] and PS93/025[41] (green) from the NE Greenland Shelf, and **g** IP_{25} from Ryder19-12-GC1 (black) and Ryder19-14-GC1 (green) in the southern Lincoln Sea (this study). Where available, IP_{25} is shown normalized to TOC, otherwise the data normalized to sediment mass is shown (see respective axes). The records from the Laptev and Beaufort Sea comprise areas that today deliver sea-ice to the LIA.

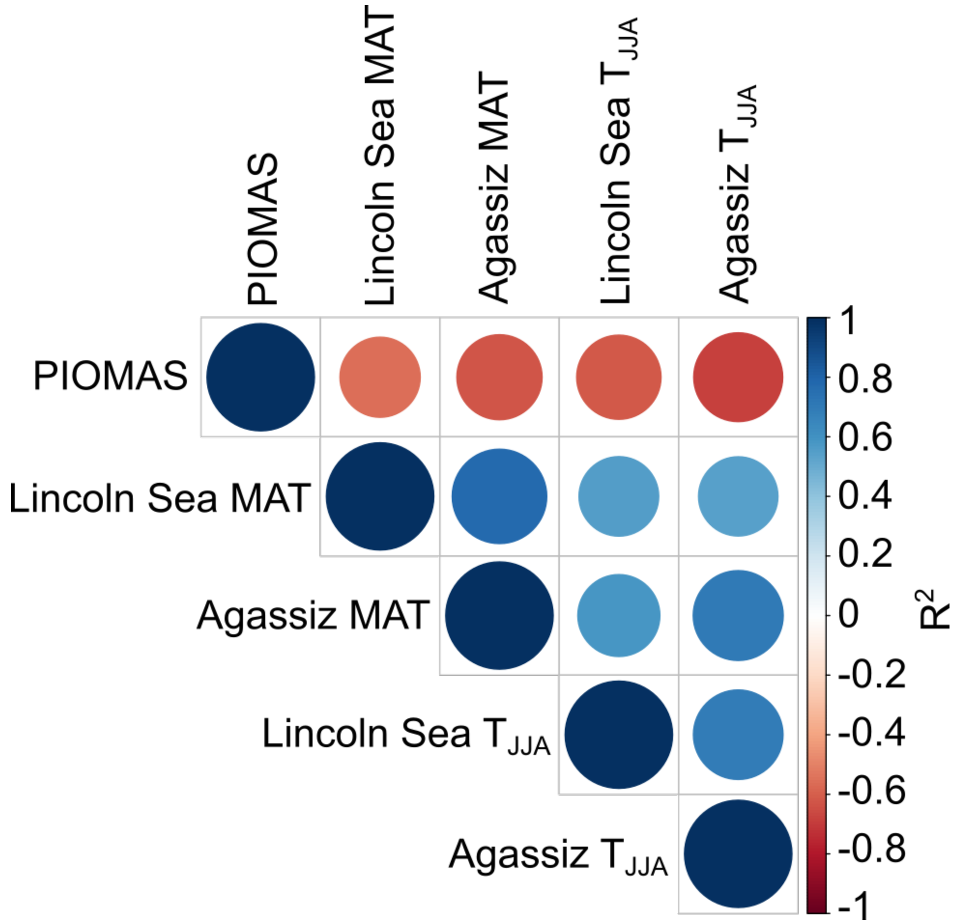

Supplementary Fig. 6. Correlation matrix of reanalysis temperature and sea-ice data from the Agassiz Ice Cap and the southern Lincoln Sea. Mean annual temperatures (MAT) and summer temperatures (T_{JJA}) at Agassiz Ice Cap (80.75 °N, 73 °W) and in the southern Lincoln Sea (82.5 °N, 55 °W) were extracted from the ERA5 reanalysis (2 m atmospheric temperatures)[48] for the period from 1979 to 2019. Annual mean sea-ice concentration in the southern Lincoln Sea (Fig. 4) for the same period was extracted from the Pan-Arctic Ice Ocean Modeling and Assimilation System (PIOMAS)[49]. The significance level for correlation is $P = 0.001$.

4. Supplementary tables

Supplementary table 1. Lithological unit (LU) boundaries in 12-GC and 14-GC.

	Ryder19-12-GC1		**Ryder19-14-GC1**	
	Bottom depth (cm)	Top depth (cm)	Bottom depth (cm)	Top depth (cm)
LU1a	68-54 and 49-0		39-35 and 33-0	
LU1b	76- 68 and 54-49		35	33
LU2	96	76	67	39
LU3a	200	96	277	67
LU3b	236	200	306.5	277
LU4	273.5	236	Not recovered	

Supplementary table 2. Overview of radiocarbon dates in gravity core 12-GC.

Laboratory ID	**Sample ID**	**Mid depth in core (cm)**	**Material**	**^{14}C age**	**Uncertainty**
OS-159557	Ryder19-12-GC1-1 13-15 cm	14	Mixed benthic foraminifera	4,940	50
OS-159558	Ryder19-12-GC1-1 23-25 cm	24	Mixed benthic foraminifera	6,480	35
OS-159559	Ryder19-12-GC1-1 33-35 cm	34	Mixed benthic foraminifera	7,100	65
OS-159560	Ryder19-12-GC1-1 63-65 cm	64	Mixed benthic foraminifera	8,100	40
OS-159561	Ryder19-12-GC1-1 93-95 cm	94	Mixed benthic foraminifera	9,720	70
OS-159544	Ryder19-12-GC1-1 103-105 cm	104	Mixed benthic foraminifera	9,370	100
OS-159562	Ryder19-12-GC1 sec. 1 113 cm to sec. 2 25 cm	135.5	Mixed benthic foraminifera	9,680	60

Supplementary table 3. Overview of radiocarbon dates in gravity core 14-GC.

Laboratory ID	Sample ID	Mid depth in core (cm)	Material	^{14}C age	Uncertainty
OS-159563	Ryder19-14-GC1-1 2-4 cm	3	Mixed benthic foraminifera	2,930	25
OS-159564	Ryder19-14-GC1-2 32-34 cm	49	Mixed benthic foraminifera	9,990	55
OS-159617	Ryder19-14-GC1-2 92-94 cm	109	*C. neoteretis*	9,530	65
OS-159618	Ryder19-14-GC1-3 12-14 cm	180	*C. neoteretis*	10,100	95
OS-152304	Ryder19-14-GC1-CC	306.5	Mixed benthic foraminifera	8,350	35

Supplementary table 4. Age-depth tie points between 12-GC and 14-GC.

Ryder19-12-GC1 Depth (cm)		Ryder19-14-GC1 Depth (cm)	Age (cal ka BP)
76	Tied to	39	8140 ± 320
200	Tied to	277	11274 ± 420

Supplementary table 5. GC-MS operating conditions and selective ion monitoring (SIM) ion masses.

Operating conditions		
Sample injection	Splitless	
Injection volume	1 µL	
Injector temperature	280°C	
Flow of carrier gas	1 mL min^{-1}	
Oven temperature profile (HBIs)	40-300 °C (10 °C min^{-1}); 8 minute isothermal interval at 300 °C; 300-320 °C (40 °C min^{-1}); 5 minute isothermal interval at 320 °C	
Oven temperature profile (sterols)	40-300 °C (10 °C min^{-1}); 12 minute isothermal interval at 300 °C	
MSD transfer line temperature	280°C	
MS ion source temperature	250°C	
Ion masses		
HBI SIM method ion masses	342.3	
	344.3	
	346.3	
	348.3	HBI II
	350.3	IP_{25}, 9-Octylheptadec-8-ene
Sterol SIM method ion masses	327.3	
	331.2	5α-androst-16-en-3α-ol
	343.3	
	382.4	
	396.4	
	458.4	
	470.4	Brassicasterol
	500.4	

Supplementary table 6. Corner coordinates of polygon in the southern Lincoln Sea in Fig. 4.

Latitude (°N)	Longitude (°W)
-60.8142	83.03249
-59.5589	82.40586
-55.1077	82.51196
-51.4459	82.74104
-47.76	83.22416
-47.9447	83.6478
-51.8858	83.90934
-59.1015	83.47041
-60.8142	83.03249

Supplementary table 7. Information on analyzed multi-corer surface samples.

Core	**Latitude**	**Longitude**	**Depth**
Ryder19-1-MC1-8	82º 19.50' N	59º 53.29' W	0-1 cm
Ryder19-2-MC1-4	82º 20.89' N	56º 56.81' W	0-1 cm
Ryder19-3-MC3-8	82º 11.33' N	51º 49.56' W	0-4 cm
Ryder19-4-MC1-6	82º 01.63' N	52º 09.60' W	0-5 cm
Ryder19-5-MC1-6	81º 59.28' N	52º 13.97' W	0-5 cm
Ryder19-6-MC2-A	82º 01.28' N	51º 44.60' W	0-5 cm
Ryder19-7-MC1-2	81º 57.03' N	51º 34.44' W	0-2 cm
Ryder19-8-MC1-4	81º 53.72' N	51º 08.25' W	0-2 cm
Ryder19-9-MC1-1	81º 53.29' N	50º 58.26' W	0-2 cm
Ryder19-12-MC1-8	82º 34.74' N	52º 31.35' W	0-2 cm
Ryder19-13-MC1-5	82º 28.63' N	54º 12.71' W	0-1 cm
Ryder19-17-MC1-1	81º 40.12' N	64º 03.43' W	0-1 cm
Ryder19-18-MC1-7	81º 00.74' N	61º 17.67' W	0-1 cm
Ryder19-19-MC1-3	80º 59.70' N	60º 58.26' W	0-1 cm
Ryder19-20-MC1-2	81º 09.11' N	62º 16.63' W	0-1 cm

5. Supplementary References

1. Belt, S. T. & Müller, J. The Arctic sea-ice biomarker IP_{25}: a review of current understanding, recommendations for future research and applications in palaeo sea-ice reconstructions. *Quat. Sci. Rev.* **79**, 9–25 (2013).
2. Lecavalier, B. S. *et al.* High Arctic Holocene temperature record from the Agassiz ice cap and Greenland ice sheet evolution. *Proc. Natl. Acad. Sci. U. S. A.* **114**, 5952–5957 (2017).
3. Stroeve, J. & Notz, D. Changing state of Arctic sea-ice across all seasons. *Environ. Res. Lett.* **13**, 103001 (2018).
4. Notz, D. & Stroeve, J. Observed Arctic sea-ice loss directly follows anthropogenic CO2 emission. *Science (80-.).* **354**, 747–750 (2016).
5. Karami, M. P., Myers, P. G., Vernal, A. de, Tremblay, L. B. & Hu, X. The role of Arctic gateways on sea-ice and circulation in the Arctic and North Atlantic Oceans: a sensitivity study with an ocean-sea-ice model. *Clim. Dyn. 2021* **1**, 1–23 (2021).
6. Vinther, B. M. *et al.* Holocene thinning of the Greenland ice sheet. *Nature* **461**, 385–388 (2009).
7. Süfke, F. *et al.* Arctic drainage of Laurentide Ice Sheet meltwater throughout the past 14,700 years. *Commun. Earth Environ. 2022 31* **3**, 1–11 (2022).
8. Prange, M. & Lohmann, G. Variable Freshwater Input to the Arctic Ocean During the Holocene: Implications for Large-Scale Ocean-Sea-ice Dynamics as Simulated by a Circulation Model. 319–335 (2004).
9. Farmer, J. R. *et al.* Arctic Ocean stratification set by sea level and freshwater inputs since the last ice age. *Nat. Geosci. 2021 149* **14**, 684–689 (2021).
10. Pieńkowski, A. J. *et al.* Seasonal sea-ice persisted through the Holocene Thermal Maximum at 80°N. *Commun. Earth Environ. 2021 21* **2**, 1–10 (2021).
11. Polyakov, I. V. *et al.* Weakening of Cold Halocline Layer Exposes Sea-ice to Oceanic Heat in the Eastern Arctic Ocean. *J. Clim.* **33**, 8107–8123 (2020).
12. Carmack, E. C. *et al.* Freshwater and its role in the Arctic Marine System: Sources, disposition, storage, export, and physical and biogeochemical consequences in the Arctic and global oceans. *J. Geophys. Res. Biogeosciences* **121**, 675–717 (2016).
13. Spielhagen, R. F., Henning, • & Bauch, A. The role of Arctic Ocean freshwater during the past 200 ky. *arktos 2015 11* **1**, 1–12 (2015).
14. Washam, P., Nicholls, K. W., Münchow, A. & Padman, L. Summer surface melt thins Petermann Gletscher Ice Shelf by enhancing channelized basal melt. *J. Glaciol.* **65**, 662–674 (2019).
15. Cai, C., Rignot, E., Menemenlis, D. & Nakayama, Y. Observations and modeling of ocean-induced melt beneath Petermann Glacier Ice Shelf in northwestern Greenland. *Geophys. Res. Lett.* **44**, 8396–8403 (2017).
16. Münchow, A., Padman, L., Washam, P. & Nicholls, K. W. The ice shelf of Petermann Gletscher, North Greenland, and its connection to the Arctic and Atlantic Oceans. *Oceanography* **29**, 84–95 (2016).

17. Cronin, T. M. *et al.* Holocene paleoceanography and glacial history of Lincoln Sea, Ryder Glacier, Northern Greenland, based on foraminifera and ostracodes. *Mar. Micropaleontol.* **175**, 102158 (2022).

18. Jennings, A. E. *et al.* Modern and early Holocene ice shelf sediment facies from Petermann Fjord and northern Nares Strait, northwest Greenland. *Quat. Sci. Rev.* **283**, 107460 (2022).

19. Jennings, A. *et al.* The Holocene History of Nares Strait: Transition from Glacial Bay to Arctic-Atlantic Throughflow. *Oceanography* **24**, 26–41 (2011).

20. O'Regan, M. *et al.* The Holocene dynamics of Ryder Glacier and ice tongue in north Greenland. *Cryosphere* **15**, 4073–4097 (2021).

21. Vincent, R. F. A Study of the North Water Polynya Ice Arch using Four Decades of Satellite Data. *Sci. Rep.* **9**, 1–12 (2019).

22. Moore, G. W. K., Howell, S. E. L., Brady, M., Xu, X. & McNeil, K. Anomalous collapses of Nares Strait ice arches leads to enhanced export of Arctic sea-ice. *Nat. Commun.* **12**, 1–8 (2021).

23. Kwok, R., Pedersen, L. T., Gudmandsen, P. & Pang, S. S. Large sea-ice outflow into the Nares Strait in 2007. *Geophys. Res. Lett.* **37**, 3502 (2010).

24. Hole, G. M. & Macias-Fauria, M. Out of the woods: Driftwood insights into Holocene pan-Arctic sea-ice dynamics. *J. Geophys. Res. Ocean.* **122**, 7612–7629 (2017).

25. Nixon, F. C., England, J. H., Lajeunesse, P. & Hanson, M. A. An 11 000-year record of driftwood delivery to the western Queen Elizabeth Islands, Arctic Canada. *Boreas* **45**, 494–507 (2016).

26. Mayewski, P. A. *et al.* Major features and forcing of high-latitude northern hemisphere atmospheric circulation using a 110,000-year-long glaciochemical series. *J. Geophys. Res. Ocean.* **102**, 26345–26366 (1997).

27. Vernal, A. de, Hillaire-Marcel, C. & Darby, D. A. Variability of sea-ice cover in the Chukchi Sea (western Arctic Ocean) during the Holocene. *Paleoceanography* **20**, PA4018 (2005).

28. Rimbu, N., Lohmann, G., Kim, J.-H., Arz, H. W. & Schneider, R. Arctic/North Atlantic Oscillation signature in Holocene sea surface temperature trends as obtained from alkenone data. *Geophys. Res. Lett.* **30**, 1280 (2003).

29. Armitage, T. W. K., Bacon, S. & Kwok, R. Arctic Sea Level and Surface Circulation Response to the Arctic Oscillation. *Geophys. Res. Lett.* **45**, 6576–6584 (2018).

30. Rigor, I. G., Wallace, J. M. & Colony, R. L. Response of Sea-ice to the Arctic Oscillation. *J. Clim.* **15**, 2648–2663 (2002).

31. Kwok, R., Spreen, G. & Pang, S. Arctic sea-ice circulation and drift speed: Decadal trends and ocean currents. *J. Geophys. Res. Ocean.* **118**, 2408–2425 (2013).

32. Jakobsson, M. *et al.* Post-glacial flooding of the Bering Land Bridge dated to 11 cal ka BP based on new geophysical and sediment records. *Clim. Past* **13**, 991–1005 (2017).

33. Dalton, A. S. *et al.* An updated radiocarbon-based ice margin chronology for the last deglaciation of the North American Ice Sheet Complex. *Quat. Sci. Rev.* **234**, 106223

(2020).

34. Ribeiro, S. *et al.* Sea-ice and primary production proxies in surface sediments from a High Arctic Greenland fjord: Spatial distribution and implications for palaeoenvironmental studies. *Ambio* **46**, 106–118 (2017).

35. Stranne, C. *et al.* The climate sensitivity of northern Greenland fjords is amplified through sea-ice damming. *Commun. Earth Environ. 2021 21* **2**, 1–8 (2021).

36. Detlef, H. *et al.* Holocene sea-ice dynamics in Petermann Fjord in relation to ice tongue stability and Nares Strait ice arch formation. *Cryosphere* **15**, 4357–4380 (2021).

37. Schweiger, A. J., Steele, M., Zhang, J., Moore, G. W. K. & Laidre, K. L. Accelerated sea-ice loss in the Wandel Sea points to a change in the Arctic's Last Ice Area. *Commun. Earth Environ.* **2**, 1–11 (2021).

38. Moore, G. W. K. & McNeil, K. The Early Collapse of the 2017 Lincoln Sea-ice Arch in Response to Anomalous Sea-ice and Wind Forcing. *Geophys. Res. Lett.* **45**, 8343–8351 (2018).

39. Moore, G. W. K., Howell, S. E. L. & Brady, M. First Observations of a Transient Polynya in the Last Ice Area North of Ellesmere Island. *Geophys. Res. Lett.* **48**, e2021GL095099 (2021).

40. Syring, N. *et al.* Holocene Interactions Between Glacier Retreat, Sea-ice Formation, and Atlantic Water Advection at the Inner Northeast Greenland Continental Shelf. *Paleoceanogr. Paleoclimatology* **35**, e2020PA004019 (2020).

41. Syring, N. *et al.* Holocene changes in sea-ice cover and polynya formation along the eastern North Greenland shelf: New insights from biomarker records. *Quat. Sci. Rev.* **231**, 106173 (2020).

42. Müller, J., Massé, G., Stein, R. & Belt, S. T. Variability of sea-ice conditions in the Fram Strait over the past 30,000 years. *Nat. Geosci.* **2**, 772–776 (2009).

43. Müller, J. *et al.* Holocene cooling culminates in sea-ice oscillations in Fram Strait. *Quat. Sci. Rev.* **47**, 1–14 (2012).

44. Hörner, T., Stein, R., Fahl, K. & Birgel, D. Post-glacial variability of sea-ice cover, river run-off and biological production in the western Laptev Sea (Arctic Ocean) – A high-resolution biomarker study. *Quat. Sci. Rev.* **143**, 133–149 (2016).

45. Fahl, K. & Stein, R. Modern seasonal variability and deglacial/Holocene change of central Arctic Ocean sea-ice cover: New insights from biomarker proxy records. *Earth Planet. Sci. Lett.* **351–352**, 123–133 (2012).

46. Stein, R. & Fahl, K. A first southern Lomonosov Ridge (Arctic Ocean) 60 ka IP25 sea-ice record. *Polarforschung* **82**, 83–86 (2012).

47. Wu, J. *et al.* Deglacial to Holocene variability in surface water characteristics and major floods in the Beaufort Sea. *Commun. Earth Environ. 2020 11* **1**, 1–12 (2020).

48. Hersbach, H. *et al.* The ERA5 global reanalysis. *Q. J. R. Meteorol. Soc.* **146**, 1999–2049 (2020).

49. Zhang, J. & Rothrock, D. A. Modeling Global Sea-ice with a Thickness and Enthalpy Distribution Model in Generalized Curvilinear Coordinates. *Mon. Weather Rev.* **131**, 845–

861 (2003).